ACS APPLIED BIO MATERIALS

www.acsabm.org Article

Near-Infrared Photoactive Theragnostic Gold Nanoflowers for Photoacoustic Imaging and Hyperthermia

Olavo Santos,[†] Juliana Cancino-Bernardi,*[,†] Paula Maria Pincela Lins, Diego Sampaio, Theo Pavan, and Valtencir Zucolotto

Cite This: https://doi.org/10.1021/acsabm.1c00519 Read Online

ACCESS | Metrics & More | Article Recommendations | Supporting Information

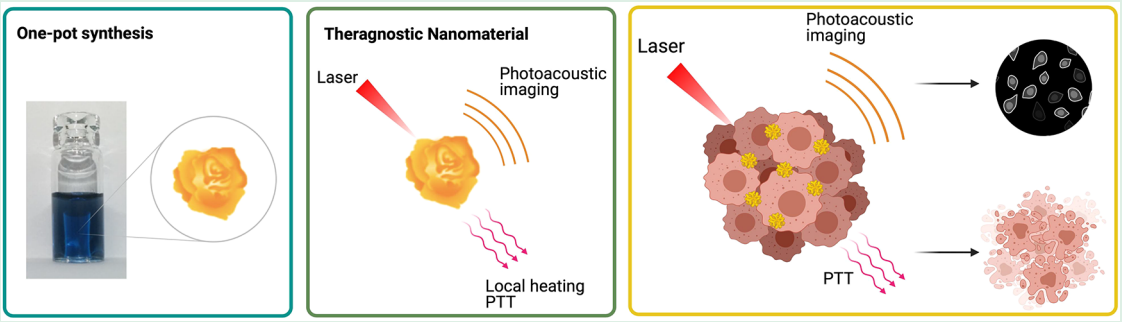

ABSTRACT: Branched anisotropic gold nanostructures present distinguished performance acting both as contrast agents for photoacoustic imaging and as active agents for photothermal therapies. Despite advances in their fabrication methods, the synthesis of such gold nanomaterials in a simple and reproducible way is still a challenge. In this paper, we report the development of branched anisotropic gold nanoparticles, the so-called gold nanoflowers (AuNFs), as near-infrared active theragnostic materials for cancer therapy and diagnosis. In situ chemical synthesis of the AuNFs was optimized to obtain monodisperse nanoflowers with controllable size and optical properties. Upon varying the temperature and gold ion concentrations, it was possible to tune the optical activity of the nanoparticles from 590 to 960 nm. The AuNFs exhibited good stability in the cell culture medium, and under laser irradiation. Photoacoustic imaging revealed that the NFs could be imaged in phantom systems even at low concentrations. In vitro tests revealed that the nanoflowers were effective in the photothermal therapy of a rat hepatocarcinoma (HTC) cell lineage. In addition, no toxicity was observed to mouse fibroblast (FC3H) cells incubated with the AuNFs. Our results reveal a simple method to synthesize branched anisotropic gold nanostructures, which is a promising platform for photothermal and photoacoustic therapies.

KEYWORDS: *gold nanoflowers, hyperthermia, theragnostics, photoacoustic imaging, nanotechnology, nanomedicine, cancer*

1. INTRODUCTION

Photothermal therapies are based on the use of light to promote heat or photochemical reaction activation as a result of light absorption in specific materials.[1,2] Photothermal applications based on laser radiation in vivo, however, may be limited by the high extinction coefficient of human tissues in the ultraviolet−visible spectrum.[3] As a result, the efficiency of the therapy can be impaired and lead to nonspecific damage because the interaction with light occurs in both diseased and healthy tissues.[3] Nanomaterials have been incorporated as active agents in photothermal applications allowing the development of minimally invasive methodologies and improving selectivity and targeting.[4] Gold-based nanoparticles (Au-based NPs), in particular, may absorb light in the near-infrared spectrum (NIR) and have been widely used as active theragnostic agents.[4] The most important characteristics of Au-based NPs are their unique optical properties, which comes mainly from their localized surface plasmon resonance (LSPR)[5] effect. This effect arises from the interaction of nanoparticles with light that, at specific wavelengths, stimulate the conducting free electrons of the particles' surface, resulting in absorption and heat generation/dissipation to the environment.[6] This phenomenon, also known as hyperthermia, has been widely explored[7,8] in oncology to raise the temperature of the tumors, inducing cellular death. Nonetheless, generalized heating can cause irreversible damage to healthy tissues.[3]

The optimization of the LSPR effects in Au-based NPs is possible by using highly anisotropic particles synthesized via specific protocols, which are active in the biological window.[5] However, the synthesis of these NPs may be complex, time

Received: May 5, 2021
Accepted: August 2, 2021

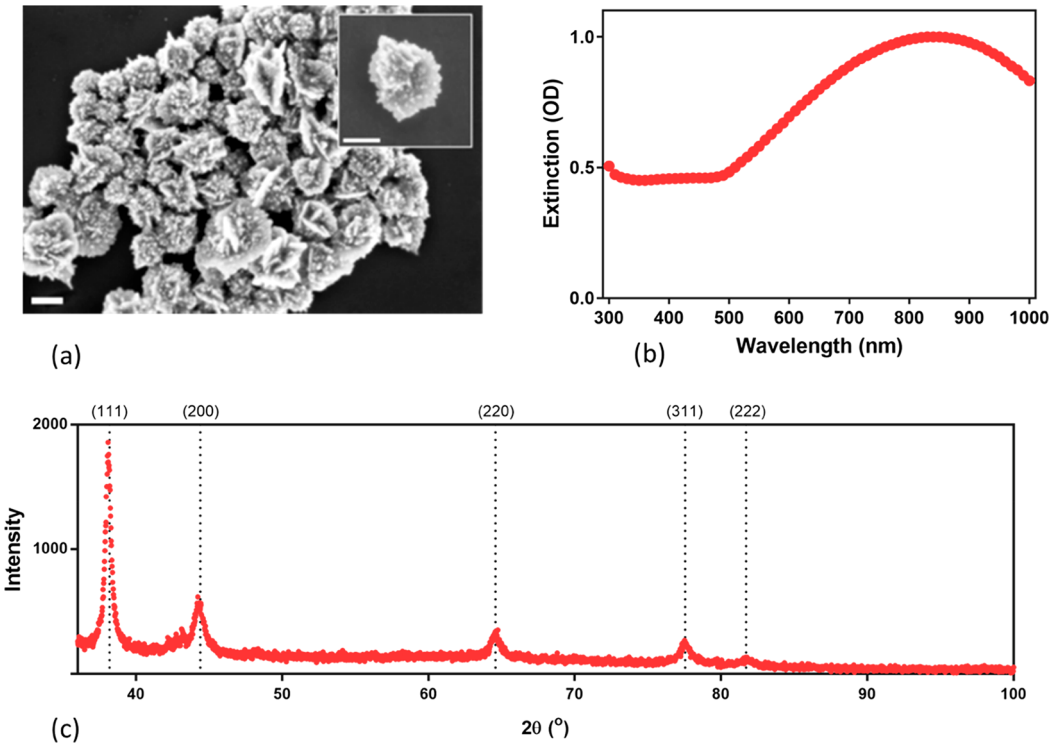

Figure 1. Characterization of AuNFs synthesized by the optimized protocol: (a) Scanning electron microscopy. The scale bars represent 100 nm. (b) UV−visible extinction spectrum. (c) X-ray diffraction spectrum.

consuming, and nonreproducible, resulting in nanoparticles with high polydispersity, compromising their large-scale production and commercial use[5,9]. In particular, branched anisotropic nanoparticles, such as the nanoflowers and nanostars[10,11], exhibit high LSPR and tunable optical activity in the NIR.[9] Given their peculiar morphology, these structures present a great enhancement of the electromagnetic field around their branches, resulting in excellent optical, electronic, magnetic, and catalytic properties[10,11]. For such nanoparticles, the LSPR effect is the result of the hybridization of plasmons associated with the nucleus and branches.[12,13] As a result, the branched nanostructures exhibit a UV−visible spectrum with an intense, wide absorption band that is usually located in the NIR.[13] In addition, their branched morphology imparts a large surface area, making them highly reactive and susceptible to heat generation.[14,15]

A wide variety of Au-based nanoparticles have already been employed as active agents for photothermal therapy.[16] In the case of AuNFs, their high absorption ratio in the NIR region makes them excellent heat generators.[14] The latter has been confirmed by several studies that validate their application for tumor hyperthermia, with therapeutic responses for a laser power density of 0.2 W/cm^2, the lowest reported pulsed lasers intensities (PW).[17] In addition, their use as active agents for photothermia has been reported, which combined with the surface-enhanced Raman spectroscopy (SERS) techniques and photoacoustic images, have allowed therapy and imaging to be carried out simultaneously.[18,19] With such a variety of geometries and sizes, the choice of nanostructures and their synthesis and modifications are fundamental in the development of nanostructures for medical applications.[20]

Herein, we report the synthesis and biomedical applications of a theragnostic Au-based NPs with absorption in the NIR. A facile one-pot synthesis was developed, producing AuNFs with homogeneous sizes and maximum tunable absorption. The AuNFs showed an excellent photoacoustic response and good photothermal conversion in the NIR region. Additionally, the AuNFs proved to be stable for long periods, maintaining their optical and physical-chemical characteristics even after two months of storage in different media and under laser irradiation. The therapeutic applications of the nanoparticles were evaluated in vitro using hepatocarcinoma (HTC) and fibroblasts (FC3H) cells by means of hyperthermia essays, in which the AuNFs exhibited higher toxicity to the tumor cells. The AuNFs proved to be promising candidates for application as theragnostic systems, as they are effective in the hyperthermia treatment of tumors with low toxicity to health cells.

2. RESULTS AND DISCUSSION

AuNF Characterization. Synthesis of the AuNFs was carried out by the reduction of gold ions using ascorbic acid in the presence of PEG-thiol as the stabilizing agent and silver ions, at room temperature. A detailed discussion on the synthetic route employed here may be found in the Supporting Information, Figures S2−S5 and Tables S1−S4.

Figure 1a shows a monodispersed branched gold nanostructure (Figure 1a) along with its UV−visible extinction spectrum featuring a broad plasmonic band centered at 850 nm (Figure 1b), characteristic of AuNFs.[21] As seen in Table 1, AuNFs with a hydrodynamic diameter of 162 nm and a zeta potential of

Table 1. Characterization of AuNFs Synthesized by the Optimized Protocol: Summary of the Physical and Chemical Characteristics of the Nanoparticles

max. extinction (nm)	hydrodynamic diameter d (nm)	PdI	zeta potential (mV)
850	162	0.101	−16

https://doi.org/10.1021/acsabm.1c00519
ACS Appl. Bio Mater. XXXX, XXX, XXX−XXX

−16 mV were obtained. The average PdI of the AuNF dispersion was very low, indicating a population of monodisperse nanostructures. Concentration of Au in AuNFs is ca. 290 μg/mL. X-ray diffraction analyses of the AuNFs revealed a face-centered cubic structure (JCPDS No. 04−0784) typical of gold nanoparticles (Figure 1c).

Stability of the AuNFs. The thermal stability of AuNFs and their stability in the culture medium were investigated. Figure S6 and the data from Table S5 showed that the AuNFs are stable in the refrigerator, maintaining their physical and chemical characteristics for more than two months of storage. An increase in temperature from 32 to 40 °C, resulted in variations in the physical-chemical characteristics of AuNFs. On the other hand, prolonged storage of AuNFs at 37 °C (body temperature) did not cause significant changes in their physical-chemical properties, as observed in Figure S7 and Table S6. In addition, the system showed no signs of aggregation when suspended in DMEM culture medium, a crucial factor for use in biomedical applications, as shown in Figure S8 and Table S7. Immersion of the AuNFs in a protein-rich medium resulted in changes in their potential zeta from −15 to −19 mV and a shift in UV spectra from 830 to 890 nm, probably due to the formation of a proteic corona. The latter may influence the biodistribution and circulation time of AuNFs in biological media.

The stability of the AuNFs under irradiation was investigated using pulsed (PW) and continuous lasers (CW) irradiation. AuNF samples were sonicated for 10 min and irradiated without dilution. For PW irradiation, a total of 3000 shots were fired with 12 mJ energy at 10 Hz. After irradiation, the AuNFs had their hydrodynamic diameter reduced by 27 nm (Table 2) and their plasmonic band shifted from 850 to

Table 2. Stability of AuNFs to Irradiation by a Pulsed Laser: Summary of the Physical-Chemical Characteristics of Gold Nanoflowers before and after Irradiation with a Pulsed Laser

before irradiation			after irradiation		
size (nm)	PdI	zeta potential (mV)	size (nm)	PdI	zeta potential (mV)
170	0.048	−23	143	0.068	−20

580 nm. Comparing the microscopies in Figure 2a, b, these changes are linked to the severe morphological changes suffered by the particles, which have lost their ramifications and have become spherical. The change in geometry affected the optical properties of nanoparticles, the plasmonic band of has become narrow and significantly displaced in the visible region (Figure 2c). Despite considerable changes to the AuNF morphology, no changes in their crystalline profile were observed after irradiation. The peaks shown in the XRD spectrum remained unchanged, as they are characteristic of the typical face-centered cubic network of the gold nanoparticles (Figure 2d).

The morphology changes observed for the AuNFs occurred probably because of the large amount of energy delivered by the nanosecond PW lasers (12 mJ of energy), which caused an increase in the temperature of the nanoparticles, heating them to the melting temperature (ca. 300 °C[22]), at which they tend to restructure into a more stable thermodynamically morphology. The latter was also highlighted by Emelianov and coauthors that observed a lower melting to silica-coated gold nanorods and gold-based nanospheres to occur at lower temperatures than that of the metal.[23] When considering photoactivated applications, such changes are undesired, as the plasmonic band is displaced outside the biological windows and can significantly affect the interaction of the nanoparticles with the biological environment.

To evaluate the stability of the particles under irradiation from a CW laser, we irradiated the samples for 1,5 h under 2.42 W/cm^2 irradiation. Figure 3 shows that the irradiation did not result in significant variations in the physical-chemical characteristics of AuNFs, as confirmed by the microscopies of Figure 3a, b. Even after a long period of irradiation, the geometry of the nanoparticles remained unchanged.

Upon CW irradiation, an increase in the AuNF dispersion temperature of ca. 10 °C was observed (Figure 3c, d). To better understand the stability of the AuNF photothermal response, we repeated the experiment with a 10× diluted dispersion of AuNFs, with a final concentration of 23.8 μg/mL. First, three consecutive irradiation cycles were performed, where the solution was irradiated for 12 min and allowed to cool to room temperature (Figure 3c). The AuNF dispersion presented a consistent cyclic temperature variation profile, with small variations between the maximum temperatures. Such variations may be related to small differences in the initial temperature.

The stability of the photothermal signal over a long period of irradiation was evaluated (Figure 3d). The diluted dispersion was irradiated for 1 h and 42 min with a 2.42 W/cm^2 CW laser. After reaching a maximum value, the system temperature was kept relatively constant until the laser was turned off. The temperature variations observed may be related to instabilities in the experimental setup, as fluctuations in the laser power. The AuNF dispersion has a maximum temperature increase of 8.8 °C was reached after about 45 min, but one may observe that after 4 min, the system had already reached an increase of 5.0 °C. Considering an initial temperature of 37 °C, such an increase would be enough to reach the hyperthermia regime, which requires temperatures between 43 and 48 °C.

Photothermal Response. We investigated the application of AuNFs as therapeutic agents in tumor hyperthermia in three stages: photothermal response, cell−nanoparticle interaction, and their efficiency to cause cell death. Our results showed that nanoparticles were stable under CW laser irradiation, and thus, a CW diode laser with a wavelength of 808 nm was used for hyperthermia, which was adjusted using an optical system to radiate a circular area of 0.32 cm^2. The system was turned on 20 min before the experiments. AuNFs were resuspended in cell culture medium with 10% FBS and sonicated for 10 min. The system was left to stand for 6 h before use in the experiments to simulate the incubation period of the nanoparticles.

Figure 4a shows the laser irradiation at 2.42 W/cm^2 of a dispersion containing 23.8 μg/mL of AuNFs and a solution containing only culture medium, for 12 min. Although an increment in the temperature of the sample containing only culture medium is observed, there is a considerably increase in the nanoflowers dispersion, which reached a 67% higher final temperature. In addition, the AuNF dispersion had their temperature raised to the desired hyperthermia region, with a final increase of 9.8 °C. To establish a protocol for in vitro therapy, we verified the dependence of the photothermal

https://doi.org/10.1021/acsabm.1c00519
ACS Appl. Bio Mater. XXXX, XXX, XXX−XXX

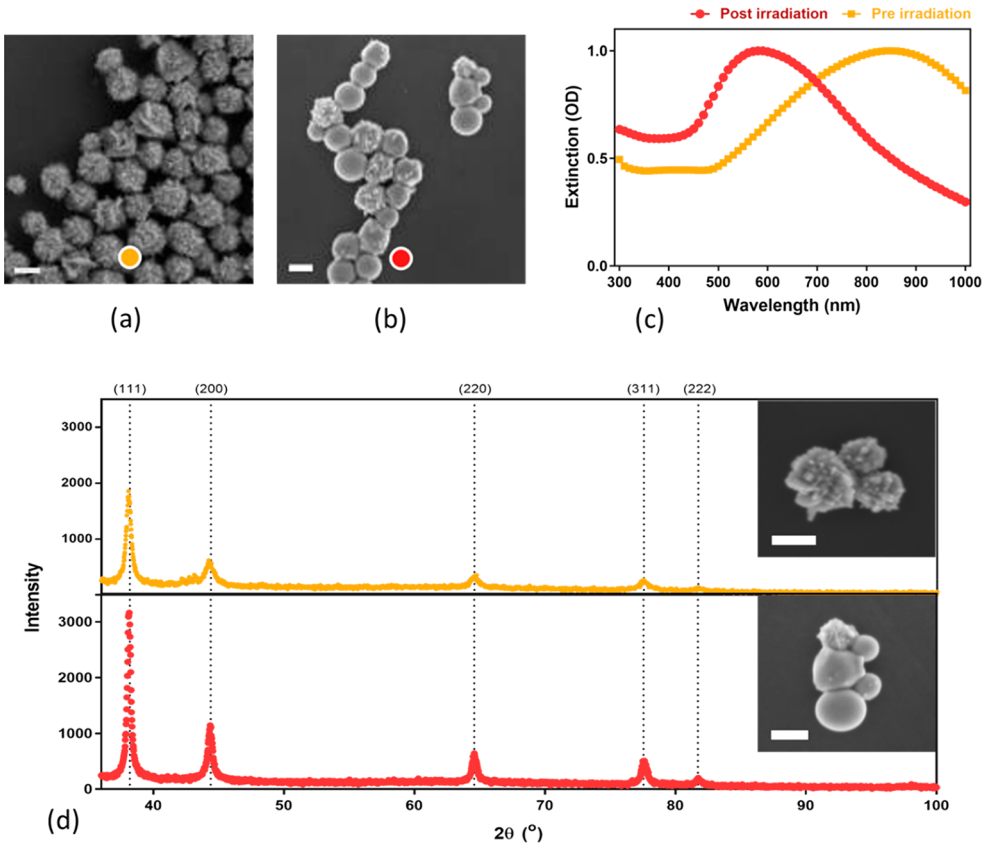

Figure 2. Stability of AuNFs to irradiation by a pulsed laser: Scanning electron microscopy (a) before and (b) after irradiation of AuNFs by a pulsed laser. (c) Extinction spectrum of pre (yellow) and post (red) irradiation gold nanoflowers. (d) X-ray diffraction spectrum of the pre (yellow) and post (red) AuNFs. Insets are scanning electron microscopy images that show morphological changes in AuNFs. The scale bars of the microscopies of a, b, and d are 100 nm.

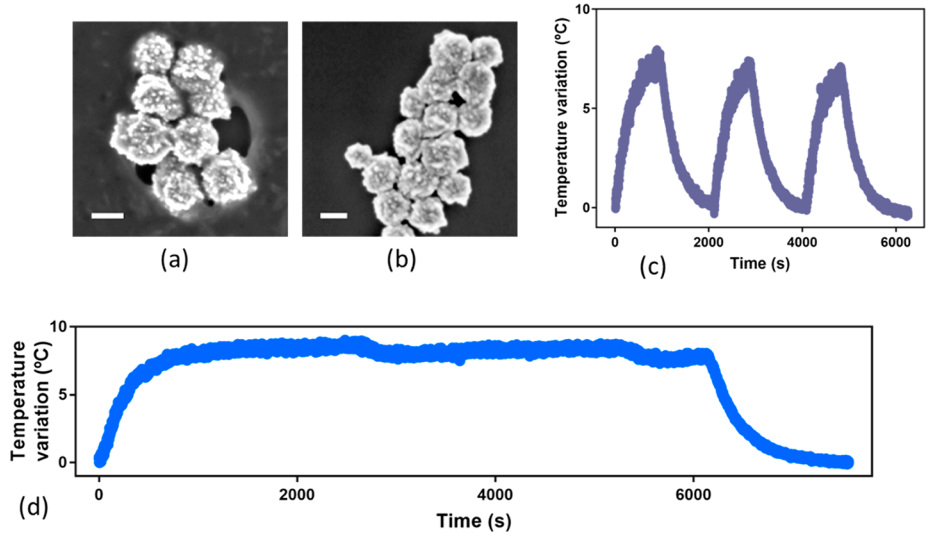

Figure 3. Stability of AuNFs to irradiation by a continuous laser: Scanning electron microscopy (a) before and (b) after irradiation of AuNFs by a CW laser. The scale bars represent 100 nm. (c) Dependence on temperature variation by the number of irradiation cycles. (d) Stability of temperature variation over time. For b, c, and d, a solution of AuNFs with a concentration of 23.8 μg/mL irradiated with 2.42 W/cm^2 was used.

response of AuNFs on the laser power and particle concentration.

To investigate the influence of the irradiation power on the temperature increase, we prepared AuNF dispersions of 23.8 μg/mL and monitored their photothermal response for irradiations at 0.73, 2.42, and 5.95 W/cm^2 for 10 min. Figure 4b shows that the irradiation at 0.73 W/cm^2 produced an insufficient heating, raising the temperature by only 1.7 °C. When irradiated with 2.42 and 5.95 W/cm^2 of laser powers, the systems were taken to the hyperthermia region (as highlighted in the figures), resulting in an increase in the temperature of 8.2 and 16, 1 °C, respectively. The irradiation

https://doi.org/10.1021/acsabm.1c00519
ACS Appl. Bio Mater. XXXX, XXX, XXX−XXX

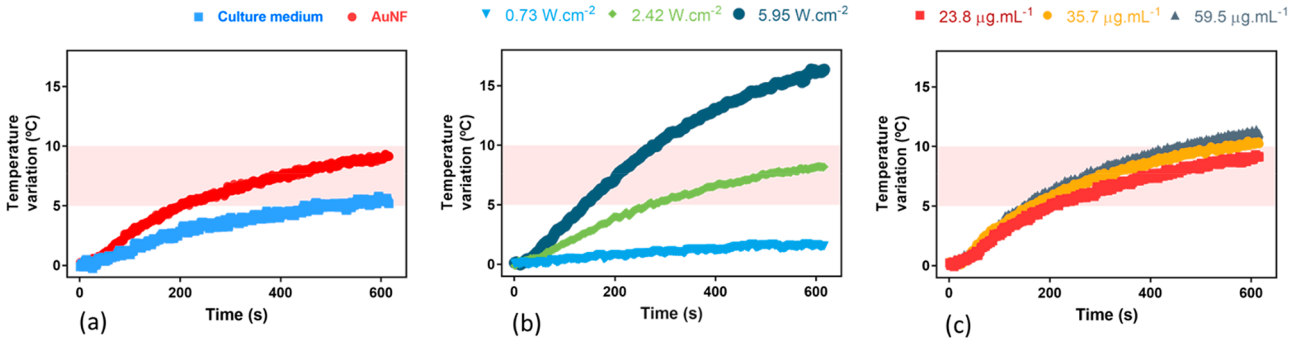

Figure 4. Photothermal response of AuNFs: (a) Irradiation of solutions containing 23.8 μg/mL of nanoparticles (light red) and containing only culture medium (blue) with 2.42 W/cm^2. (b) Irradiation of solutions with 23.8 μg/mL with 0.73 (light blue), 2.42 (green), and 5.95 W/cm^2 (dark blue). (c) Irradiation of solutions containing 23.8 (red), 35.7 (yellow), and 59.5 μg/mL (gray) with 2.42 W/cm^2. The highlighted region represents the hyperthermia region considering an initial temperature of 38.0 °C.

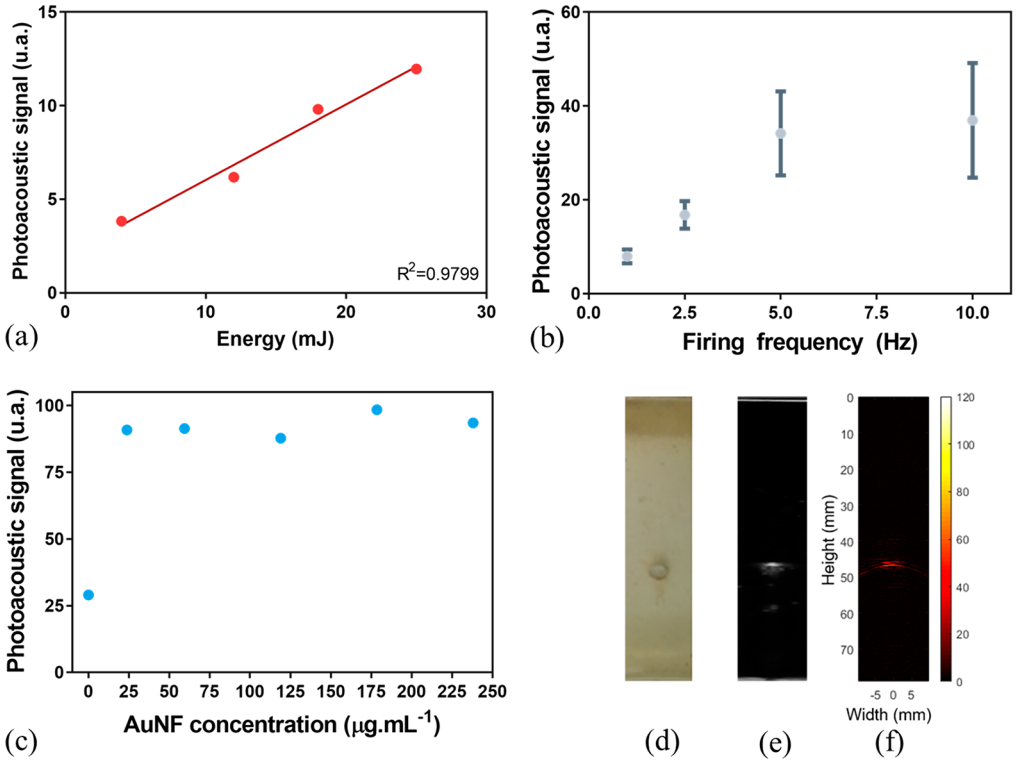

Figure 5. Photoacoustic characterization of AuNFs: (a) Dependence of the photoacoustic signal on laser power. (b) Dependence of the photoacoustic signal on the laser firing frequency. (c) Dependence of the photoacoustic signal AuNF concentrations. The experiments were performed based on variations of the standard protocol that used a power of 12 mJ at a wavelength of 770 nm with a firing frequency of 10 Hz and nanoparticle solutions with a concentration of 238 μg/mL. The error bars in a and b represent the standard deviation of 10 shots. Photoacoustic image of AuNFs: (d) Front photo of the phantom used for photoacoustic measurements. (e) Ultrasound image obtained from the phantom. (f) Photoacoustic image of the nanoparticles at 770 nm obtained with a solution containing 23.8 μg/mL of AuNFs and irradiation with energy of 12 mJ and pulse repetition frequency of 10 Hz.

of the system at 2.42 W/cm^2 led the system to reach the desired hyperthermia region after 4 min and 25 s. For the highest laser power density (5.95 W/cm^2), however, the system reached the condition of hyperthermia after 2 min and 20 s. Thus, the laser power density of 2.42 W/cm^2 is more appropriate and safer for therapy, as it keeps the system, at the concentration used, for a longer period of time in the hyperthermia region.

The dependence of the photothermal response on the concentration of AuNFs was evaluated by irradiating the AuNF dispersions at 23.8, 35.7, and 59.5 μg/mL concentrations, representing dilutions of the stock dispersion of 10, 15 and 25%, respectively. As observed in Figure 4c, the dispersions reached a maximum temperature increase of 9.3, 10.2, and 11.3 °C, reaching the hyperthermia regime after 3 min and 21 s, 2 min and 43 s, and 2 min and 28 s, respectively for the 23.8, 35.7, and 59.5 μg/mL concentrations. Under irradiation, the AuNF dispersions at concentrations of 35.7 and 59.5 μg/mL remained in the desired temperature region for 6 min and 7 s and 4 min and 52 s. On the other hand, irradiation of the dispersion at 23.8 μg/mL did not cause the temperature to exceed the hyperthermia region upper limit, keeping the system in the condition of hyperthermia for 6 min and 55 s.

https://doi.org/10.1021/acsabm.1c00519
ACS Appl. Bio Mater. XXXX, XXX, XXX−XXX

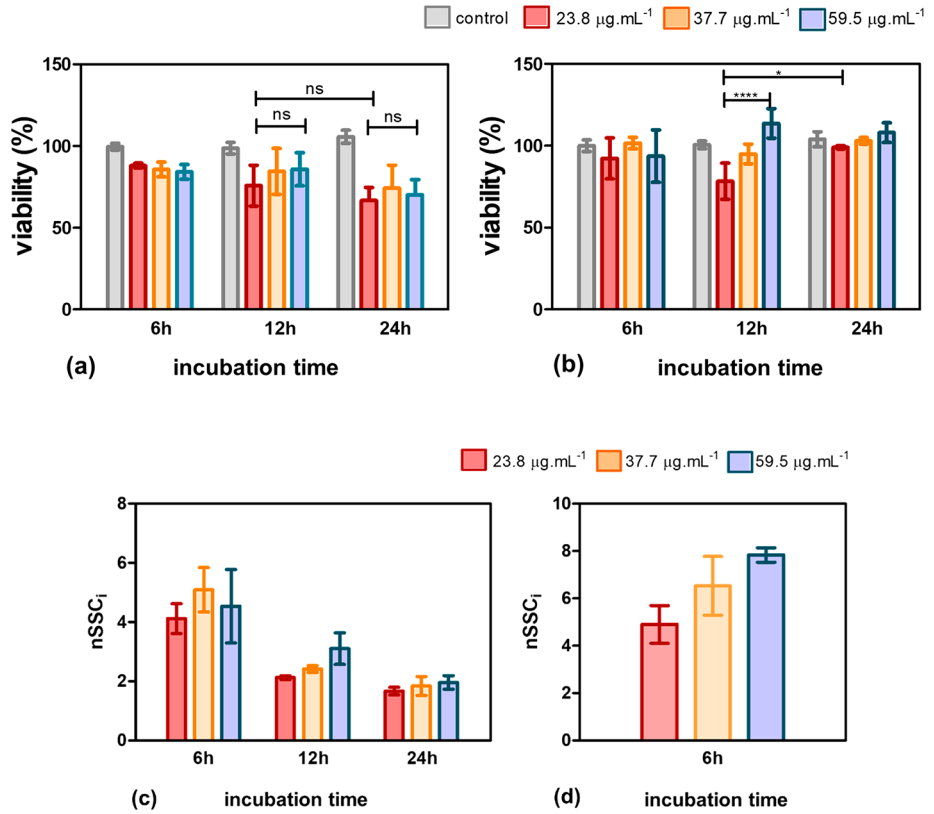

Figure 6. In vitro toxicity of AuNFs at 23.8, 35.7, and 59.5 μg/mL after 6, 12, and 24 h of incubation in (a) HTC tumor cells and (b) FC3H healthy cells. Uptake of AuNFs in vitro: Flow cytometry side scattering ($nSSC_i$) intensity in (c) HTC cells and (d) FC3H cells after exposure to AuNFs. The $nSSC_i$ values was obtained by divided the SSC of each cell sample by the SSC of the control group without AuNF. The error bars represent the standard deviation of three repetitions. The values were assigned with statistical significance at $P < 0.05$; indicated confidence values are 95%* or 99.9%*** (ANOVA one-way/Tukey). ns means not statistically significant values.

Photoacoustic Images. The photoacoustic imaging technique is based on the generation of acoustic waves by thermal expansion, which is time dependent. To establish a protocol for the acquisition of photoacoustic images, we carried out a study to verify the ability of AuNFs to produce photoacoustic signals. A characterization of the photoacoustic response was evaluated in terms of the laser power, the laser pulse frequency, and the nanoparticle concentrations. The photoacoustic protocol was established as an energy of 12 mJ, a pulse frequency of 10 Hz, and a concentration of 238 μg/mL AuNFs.

According to Figure 5a, the AuNF photoacoustic response showed a linear dependence on the excitation energy in the energy range studied from 4 to 28 mJ. The dependence of the photoacoustic signal on the laser pulse repetition frequency was also evaluated. The photoacoustic signal was monitored for different laser frequencies, viz., 1.0, 2.5, 5.0, and 10.0 Hz. As seen in Figure 5b, the signal linearly increased between 1 and 5 Hz. However, some fluctuation in the response was observed between 5 and 10 Hz. The latter can be associated with the increase in the excitation frequency that promotes a greater temperature variation due to the absorption and conversion of heat energy by AuNFs. However, the system exhibits an energy conversion limit that is reached when the excitation frequency increases. Thus, the frequency of 10 Hz was used for the other experiments. Finally, the dependence of the photoacoustic signal on the AuNF concentration was verified. No significant variations in the photoacoustic signal were observed (Figure 5c).

Photoacoustic images were obtained using the optimized parameters of AuNF concentration of 23.8 μg/mL, excitation at 770 nm, frequency of 10 Hz, and laser energy of 12 mJ. The experiment was carried out by placing the AuNF dispersion in the cylindrical inclusion in the center of the phantom (Figure 5d). Using the pulse-echo mode, the position of the inclusion inside the phantom was visualized within the ultrasound image (Figure 5e). The image is formed based on the signal from the AuNFs, using the photoacoustic mode. Figure 5f shows that AuNFs produced a significantly high photoacoustic signal, resulting in a clear image of their location inside the phantom. The photoacoustic signal resulted in a contrast with low background noise, making it easy to identify the location of the nanoparticles in the image. The AuNFs produced considerably high photoacoustic signals, even at low concentrations, a fundamental characteristic for in vivo applications, in which only a fraction of the nanoparticles is internalized by the tumor.

In addition to hyperthermia, the photothermal conversion of NIR Au-based NPs can also be used to obtain images, as is done in the photoacoustic technique (PA).[24] Using laser pulse sequences, heating and cooling cycles are induced which, because of a thermoelastic expansion of the tissues, produce acoustic waves that can be detected using an ultrasound transducer.[25] However, most tissues present a low photoacoustic contrast, making them indistinguishable through the technique. Thus, through the heating generated by the AuNFs, the photoacoustic signal generated is considerably accentuated,

https://doi.org/10.1021/acsabm.1c00519
ACS Appl. Bio Mater. XXXX, XXX, XXX−XXX

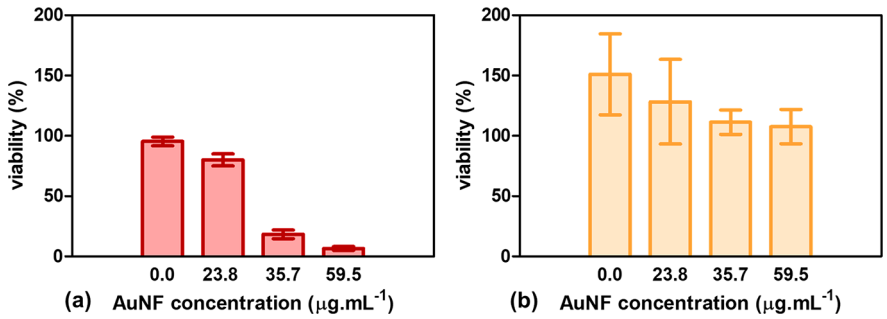

Figure 7. Viability of the (a) tumor (HTC) and (b) healthy (FC3H) cells after laser irradiation in the presence of 0, 23.8, 35.7, and 59.5 μg/mL AuNFs. The samples were incubated for 6 h and irradiated for 12 min by a CW laser at 2.42 W/cm^2. The error bars correspond to the standard deviation obtained from three experiments.

making them excellent candidates to act as contrast agents for PA modalities.[26]

AuNF−Cell Interaction and Therapeutic Efficiency. The interaction of the AuNFs with cells was performed to assess their toxicity and uptake features. The toxicity of AuNFs was monitored over a 24 h period, in which healthy and tumor cells were treated with AuNFs at concentrations of 23.8, 35.7, and 59.5 μg/mL. Cell viability was verified by colorimetric tests after 6, 12, and 24 h of incubation. All experiments were carried out in triplicate. Figure 6 shows that the incubation of the cells with AuNFs produced effects in both the tumor and healthy cells. The viability of the tumor cells reduced by 35% after 24 h (Figure 6a). We also observed that the toxicity did not have a direct relationship with the concentration of the AuNFs, showing similar viability for all concentrations employed. On the other hand, tests with healthy cells showed no signs of toxicity for all concentrations employed (Figure 6b). The statistical analysis of the viability results from the cancer cell lines has no statistical relevance by any conditions.

To confirm AuNF uptake, we carried out a study based on the granularity of the cells, analyzed by side scattering via flow cytometry (nSSC$_i$), that is the SSC of each signal divided by the control cell group which was without ANFs. As reported in the literature,[27] there is a direct relationship between the number of nanoparticles internalized and the granularity of cells. To assess the internalization of AuNFs, we monitored the nSSC$_i$ of tumor cells for 24 h for cells incubated with AuNFs at concentrations of 23.8, 35.7, and 59.5 μg/mL. Tests were performed in triplicate.

Figures 6c, d reveal the uptake of the nanostructures in both tumoral and healthy lineages. A direct relationship between uptake and AuNF concentration is observed. Figure 5c shows that AuNF internalization is higher for shorter incubation times, which may be related to the time-dependent changes occurring on the nanoparticles's surface, as a result of the protein corona formation.

The therapeutic efficiency of AuNFs toward hyperthermia experiments was assessed. Tumor and healthy cells were incubated with AuNF dispersions at 23.8, 35.7, and 59.5 μg/mL concentrations for 6 h. The cells were irradiated by a 2.42 W/cm^2 CW laser line at 808 nm for 12 min.

The experiments were carried out in triplicate. Figure 7 shows that the hyperthermia experiments using AuNFs were selective, as they were efficient at inducing cell death in the tumor cell lines (Figure 7a) and not reducing the viability of healthy cells (Figure 7b). The irradiated tumor cells showed a significant reduction in cell viability for all nanoparticle concentrations. At the lowest concentration, the average viability was 76.4%, whereas for cells treated with AuNF concentrations of 35.7 and 59.5 μg/mL, the cells population was reduced to 17.2 and 8.6%, respectively. For comparison, the cell viability observed in the toxicity tests for 6 h of incubation was 88.4, 85.9, and 84.5% for AuNF dispersions at 23.8, 35.7, and 59.5 μg/mL (Figure 5a). The latter results corroborate the efficient hyperthermia response of AuNFs toward tumor cell lines.

Corroborating the toxicity results from Figure 6b, the viability of the healthy cells was not affected by the phototherapy, probably because healthy cells are more resistant to temperature variations.[28] The viability values higher than 100% indicate that the cells proliferated more, which means that the presence of nanoparticles did not influence the cell proliferation. Even for FC3H cells treated with AuNFs at a concentration of 59.5 μg/mL, the viability remained above the reference, indicating that the lineage was not affected by the therapy. Overall, the particles showed great efficiency in the therapy of the tumor cell line (HTC), showing a reduction of up to 91.4% of cell viability after irradiation with the CW laser. The intracellular plasmonic literature shows a shift dependence of the LSPR Au-based NP band and its subcellular compartment localization. Some studies revealed a band shift of almost 40 nm once they were inside or outside cells[29,30] Although this intracellular plasmonic effect probably did not alter the PTT property of our AuNF because of their broad NIR band, as observed in PTT results. The shift in the plasmonic band was expected because of the differences in the dielectric environment, as highlighted by Evans et al. in a SERS study.[31]

It is important to emphasize that Au-based NIR nanoparticles that respond to light in the NIR range of 650−950 nm can prevent damage to surrounding healthy tissues as well as enable sufficient light depth of penetration in tissues to provide sufficient photothermal efficiency.[32] In this context, healthy cells are resistant to photothermal therapy, as observed in Figure 7b. Although AuNFs had no specificity-based surface modification, the enhanced permeability and retention (EPR) effect of cancer cells encourages it. Traditionally, EPR-mediated tumor accumulation is proposed to result from long-circulating nanoparticles with a hydrodynamic diameter size exceeding the renal clearance threshold, which can extravasate from leaky tumor vessels. Some authors focused on the applications of physical strategies to improve the EPR effect of tumors including ultrasound and hyperthermia, just using passive nanoparticles, as observed in this study.[33]

As observed in this study, the LSPR effect of metal NPs is an essential aspect to allow their application in hyperthermia. The latter is possible because of the interaction of NPs with light

https://doi.org/10.1021/acsabm.1c00519
ACS Appl. Bio Mater. XXXX, XXX, XXX−XXX

Scheme 1. Synthesis of AuNFs: (a) Schematic Drawing of the Nanoparticle Synthesis Process; (b) Final Nanoparticle Dispersion; (c) Scanning Electron Microscopy of the AuNFs[a]

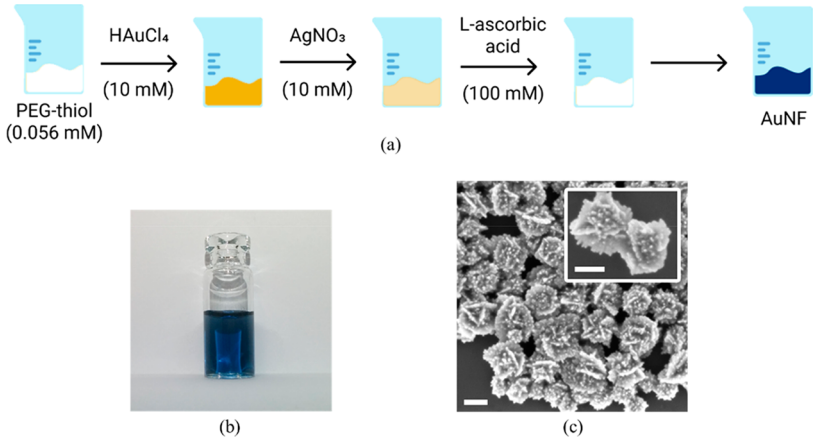

[a]The scale bars represent 100 nm.

that, at specific wavelengths, stimulate the electrons on their surface to oscillate, resulting in the dissipation of heat to their environment.[6] The heating response of plasmonic AuNPs has been extensively studied in function of shape and size.[32] In fact, plasmonic NPs that have NIR absorption allow their application of the photothermal effect with a minimum loss of radiation due to tissue adsorption, which means that they overcome the strong absorption of tissues in the UV−vis region.[34,35]

Herein, we demonstrated that AuNFs were efficient nanosources of heat because of their efficient interaction with light, which results in the conversion of the absorbed photons into heat to hyperthermia and photoacoustic therapies. Along with the LSPR effect, the ideal NP to PTT should also (i) be a uniform size and shape; (ii) interact with NIR light in the range of 700−1000 nm to prevent health tissue damage and enable depth of penetration; (iii) be photostable in aqueous solution and (iv) have low or no cytotoxicity[36,32].

Although the potential use of NIR Au-based NPs in both therapies is increasing, most photothermal studies make use of laser powers that are higher than the maximum permissible exposure of skin as per ANSI regulations (0.4 W cm^{-2} at 850 nm), one of the disadvantages in our study. The efficiency and the laser power are strictly dependent on the NP concentration into the cells, it means that these characteristics should be combined with optimized cellular uptake. The lowest laser power irradiance published until now is 0.2 W cm^{-2} that was reported in photothermal therapy to treat prostate cancer cells using gold nanostars.[37] On the other hand, a laser power of 4.2 W cm^{-2} was combined with gold nanocrosses for 30 s to induce shrinkage and collapse in cancer cells with efficient photothermal results.[35] In this context, to improve the applicability of hyperthermia and photoacoustic in human therapies, the field should overcome such a problem.

3. CONCLUSION

The synthetic route proposed here proved to be efficient in the preparation of anisotropic AuNFs, providing a simple and reproducible method to obtain monodispersed nanoparticle systems. The nanoparticles were stable over a long period of time, showing small variations in their physicochemical properties after more than two months of storage. Changes in the AuNF morphology was also observed for high temperature treatments, as imposed by the irradiation with PW lasers. In contrast, the AuNFs exhibited great physicochemical and photothermal stability when irradiated by a CW laser line. The irradiation of the AuNFs produced a significant temperature increase, sufficient to lead the system to a hyperthermia temperature regime. The AuNFs showed great therapeutic potential for use as active agents for hyperthermia and photoacoustic imaging, exhibiting low in vitro toxicity when not irradiated and good therapeutic efficiency under irradiation, as revealed by the cell viability decrease of up to 91.4% for the HTC tumor cells. In addition, the nanoparticles exhibited specificity toward tumor cells, showing no toxicity to the healthy cells, even without any surface modification. In summary, we present a monodispersed one-pot synthesis fabrication of stable nanostructures with complex morphology and with promising performance in diagnostics and therapy.

4. EXPERIMENTAL SECTION

Materials. All reagents were used as purchased and solutions were prepared using ultrapure water (18.2 MΩ cm at 25 °C). Tetrachloroauric acid ($HAuCl_4 \cdot 3H_2O$), L-ascorbic acid, silver nitrate ($AgNO_3$), poly(ethylene glycol) methyl thiol (MW = 10 000) (PEG-thiol), sodium hydroxide (NaOH), and trypan blue were acquired from Sigma-Aldrich (Brazil). Culture media Dulbecco's modified Eagle's medium (DMEM), fetal bovine serum (FBS), and trypsin solution were purchased from Vitrocell (Campinas, Brazil).

Glassware and magnetic bars used were cleaned before each experiment using a fresh aqua regia solution (HCl and HNO_3 in 1:3 ratio). In addition, reagents used in cell cultures were previously autoclaved and the procedures performed in a laminar flow chamber using sterile materials.

Synthesis of the Gold Nanoflowers. The AuNF synthesis was carried out based on variations in the following protocol. Initially, 35 μL of $HAuCl_4$ (10 mM) was added to 1 mL of a solution of PEG-thiol (0.056 mM). Then, 15 μL of $AgNO_3$ (10 mM), and 150 μL of L-ascorbic acid (100 mM) were added to the solution. Throughout the procedure, the dispersion was kept at 23 °C and stirred at 400 rpm by a magnetic bar. After 5 min, 100 μL of a PEG-thiol solution (0.448 mM) was added and the dispersion was kept under sonication for 30 min. Finally, the final dispersion was placed under mild agitation overnight at 4 °C. A highlight of the synthesis process is shown in Scheme 1.

AuNF Characterization. The extinction measurements were carried out for samples placed in a quartz cuvette with 1 cm of optical

https://doi.org/10.1021/acsabm.1c00519
ACS Appl. Bio Mater. XXXX, XXX, XXX−XXX

path using a SpectraMax M3 UV−visible spectrophotometer (Molecular Devices) in the range of 300−1000 nm. Extinction values of the same cuvette containing ultrapure water or culture medium were subtracted as baselines. Hydrodynamic size measurements and the state of aggregation of the nanoparticles were carried out in situ by dynamic light scattering (DLS) using a Zetasizer Nano ZS-90 (Malvern). The measurements were obtained upon irradiation at 632.8 nm at 25 °C, with a detector positioned at 90° in relation to the incident beam. The DLS measurement of each sample was carried out in triplicate. Zeta potential measurements were also obtained using the Zetasizer Nano ZS-90 (Malvern), featuring a disposable polycarbonate cell with gold-plated metal contacts, specifically for zeta potential analysis. The samples were analyzed in triplicate, at 25 °C.

Morphology analysis of AuNFs was performed by scanning electron microscopy with field emission (FEG-SEM). Silicon substrates (Sigma-Aldrich) were cleaned using acetone, isopropanol, ethanol, and water in an ultrasound bath for 10 min each and then dried using flowing nitrogen. After cleaning, the samples diluted in ultrapure water were placed on the substrates and dried under a vacuum in a desiccator, where they remained for 12 h. The images were then obtained using a Zeiss Sigma VP FEG-SEM at 3 kV in high vacuum mode. To obtain the X-ray diffraction spectra (XRD), we synthesized and centrifuged 10 mL of AuNFs at 4 °C for 10 min at 7800 *g*. The supernatant was discarded and the AuNFs resuspended in 1 mL of ultrapure water. The dispersion was then vacuum-dried in a desiccator over a glass coverslip. The samples were analyzed using a Rigaku Rotaflex RU200B X-ray unit, with a voltage of 40 kV and 60 mA with Cu anode. A normal scan of 5−100° with a step of 0.0200/s and speed of 1°/min was used. Finally, the vibrational spectrum in the near-infrared (FTIR) was obtained using an iS50 spectrophotometer (Nicolet) in the range of 400−4000 cm^{-1}, with a resolution of 4 cm^{-1}. Each spectrum was obtained from an average of 128 measurements in the transmittance mode. For FTIR measurements, the samples were vacuum-dried in a desiccator and then mixed with KBr in the proportion of 1:80 and pressed, forming tablets of 0.5 cm in diameter.

Photothermal Response. A stock dispersion of AuNFs was sonicated and centrifuged for 10 min at 7800 g at 4 °C, respectively. The AuNFs were resuspended in culture medium and stored for 6 h. Dispersions with appropriate concentrations were prepared in portions of 500 μL. The samples were then irradiated in a transparent quartz cuvette using an 808 nm continuous laser (CW) (iZi, LASERline) power of 2.42 W/cm^2 with a circular area of 0.32 cm^2. The temperature of the dispersion was monitored using an optical thermometer (FOT Lab Kit Fluoroptic Thermometer, LUXTRON). The initial temperature of the measurements was maintained at approximately 23 °C. The AuNF concentration was estimated on the basis of the dry samples. Briefly, 1 mL of the AuNF dispersion was placed in a container of known weight and set to dry for 12 h in an oven at 60 °C. Once dry, the samples were weighed and the concentration obtained. All measurements were performed in triplicate.

The effect of temperature on the stability of the AuNFs due to the photothermal response was evaluated by both monitoring the NF hydrodynamic diameter and the polydispersity index using a Zetasizer Nano ZS-90 (Malvern) equipment with temperature control. Briefly, an AuNF dispersion was diluted 10× in ultrapure water and its hydrodynamic diameter was monitored between 23 and 60 °C, with a 2 °C step. The measurements for each temperature were performed in triplicate. The monitoring of the UV−visible extinction spectrum was performed using a SpectraMax M3 UV−visible spectrophotometer (Molecular Devices) with temperature control. The spectrum was obtained between 300 and 1000 nm, in a quartz cuvette of 1 cm of optical path, with an AuNF dispersion without dilution, between temperatures of 23 and 60 °C, with a step of 2 °C. Extinction values of the ultrapure water were subtracted as baselines.

Interaction of the AuNFs with Biological Environment. To assess the interaction of the AuNFs with biological medium, we sonicated the stock dispersion for 10 min and centrifuged aliquots at 4 °C for 10 min at 7800 *g*. The translucent supernatant was discarded and the AuNFs were resuspended in ultrapure water or culture medium. The samples were then sonicated for 10 min, gently agitated at 38 °C for 16 h, and centrifuged again under the same conditions. After resuspension, AuNFs were sonicated for 10 min and characterized.

Pulsed Laser (PW) and Continuous Laser (CW) Irradiation. The optical stability of AuNFs was verified using a Brilliant B Quantel (850 mJ) pulsed laser system with a Rainbow OPO system (Quantel). Samples containing 1 mL of AuNF dispersion were irradiated by 1000 laser pulses with 12 mJ of energy at 770 nm, with a pulse repetition frequency of 10 Hz and 5 ns pulse duration. The irradiated dispersion was then characterized by DLS, UV−visible spectroscopy, zeta potential, and SEM. To check the AuNF stability under irradiation from a CW laser, we sonicated the AuNF stock dispersion for 10 min and removed an aliquot. The sample was then irradiated in a transparent quartz cuvette using an 808 nm CW diode laser (iZi, LASERline) with a circular area of 0.32 cm^2 with 2.42 W/cm^2 for 1 h and 42 min. The irradiated solution was then properly diluted and characterized by DLS, UV−visible spectroscopy, zeta potential, and SEM.

Photoacoustic Spectroscopy and Imaging. The photoacoustic imaging of AuNFs was performed using a phantom manufactured according to an established protocol.[38] Briefly, 1 mL of AuNFs was introduced into a cylindrical inclusion of 0.5 cm in radius located in the center of the phantom. A gel was placed over the phantom and the ultrasound probe was carefully positioned at 90° with the inclusion, according to Scheme S1. The samples were irradiated with 600−1000 pulses at 90° using a Brilliant B Quantel laser (850 mJ) with a Rainbow OPO system that allowed the adjustment of the wavelength between 680 and 950 nm and the acoustic signal was monitored using a modified ultrasound system (Sonix RP, Ultrasonix) operating in pulse-echo or photoacoustic mode. The AuNF photoacoustic signal was monitored by variation in the excitation wavelength, the irradiation energy, and the laser repetition pulse frequency. The photoacoustic signal was monitored using 23.8, 35.7, and 59.5 μg/mL AuNF dispersion. Ultrapure water was used as baseline to photoacoustic signal.

To obtain the photoacoustic images, 1 mL of AuNF dispersion (23.8 μg/mL) was inserted into the cylindrical inclusion of the manufactured phantom. Using the setup previously described, the system was irradiated by a pulsed laser Brilliant B Quantel (850 mJ) with a Rainbow OPO system at 90° with a wavelength of 770 nm, with an energy of 12 mJ and a pulse repetition frequency of 10 Hz. The signal captured by the ultrasound system in photoacoustic mode was analyzed and plotted using an algorithm in *MATLAB*.

Cell Culture. In vitro studies were carried out using two liver cell lines, viz., mouse fibroblasts (FC3H) and rat hepatoma cells (HTC), obtained from the Rio de Janeiro Cell Bank (BCRJ). Cells were grown in DMEM culture medium supplemented with 10% FBS and maintained at 37 °C in 5% CO_2 in an incubator. Cell growth was monitored using a Nikon Eclipse TS 100 inverted microscope. Cell viability was assessed before each experiment using trypan blue exclusion assays, showing viability greater than 95%. Before use, the AuNF dispersion was sonicated for 10 min and an aliquot was removed and centrifuged at 7800 *g* for 10 min at 4 °C. The translucent supernatant was discarded and the AuNFs were resuspended in DMEM culture medium supplemented with 10% FBS. The diluted dispersion was then sonicated for 10 min to homogenize.

Cell Viability, Toxicity, and Uptake. The toxicity of AuNFs was assessed by incubation with the cell lines, followed by monitoring cell viability within 24 h. Briefly, 1×10^5 cells were seeded in 96-well plates with a final volume of 200 μL. After 24 h, the cells were incubated in triplicate with AuNF dispersions at 23.8, 35.7, and 59.5 μg/mL and a control group treated with culture medium only. The plates were incubated in an oven with an atmosphere of 5% CO_2 and 37 °C. Viability was assessed via proliferation by crystal violet after 6, 12, and 24 h using the control group for the percentage analysis. Ninety-six-well plates were used to the crystal violet assays. In this case, the culture medium was removed from the wells and the samples

https://doi.org/10.1021/acsabm.1c00519
ACS Appl. Bio Mater. XXXX, XXX, XXX−XXX

were thoroughly washed three times with sterile 1% PBS. Then, 100 μL of 70% ethanol was added and kept for 10 min to fix the culture. After removing the solution, the samples were thoroughly washed with PBS and 40 μL of crystal violet solution (0.1%) was added. The plates were incubated for 25 min and the wells are washed five times with 100 μL of PBS to remove an excess of dye. Then, 100 μL of acetic acid (10%) was added to each well and the sample plate was incubated again for 30 min. Finally, the absorbance was read in a microplate reader (SpectraMax M3, Molecular Devices) using 540 nm filters. The relative percentage of viability was calculated by the ratio of the absorbance of the treated groups to that of the control groups for each experiment.

The uptake analysis was performed based on the protocol proposed by Park and colleagues:[27] 5×10^5 cells were seeded in 24-well plates and incubated for 24 h. The samples were then incubated with 500 μL of AuNF dispersion at 23.8, 35.7, and 59.5 μg/mL and a control group containing only culture medium. After 6, 12, and 24 h, the samples were cleaned off the plate using trypsin, centrifuged, and resuspended in 250 μL of PBS. The samples were centrifuged and resuspended two more times to remove debris and excess of AuNFs from the medium. Finally, after careful homogenization, the contents of the wells were transferred to polypropylene cytometry tubes and analyzed by flow cytometry (FACSCalibur, BD), acquiring 10 000 events. Statistical analysis was performed based on the control group not being treated with nanoparticles. All experiments were carried out in triplicate.

Hyperthermia Assays. To analyze the therapeutic efficiency of AuNFs in hyperthermia assays, 5×10^5 HTC cells and 5×10^5 FC3H cells were seeded in a 96-well plate. After 24 h, culture medium was removed and the cells were treated with 200 μL of AuNF dispersion at 23.8, 35.7, and 59.5 μg/mL and two control groups treated with medium. The samples were then incubated for 6 h at 37 °C with an atmosphere of 5% CO_2 and washed twice with PBS. Finally, 100 μL of medium was added to each well and the cells were irradiated using the 808 nm CW diode laser (iZi, LASERline) with a circular irradiation area of 0.32 cm^2 and a power adjusted to 2.42 W/cm^2. After exposure to the laser for 12 min, the cells were incubated for 2 h and viability was assessed via proliferation by crystal violet assay, using an untreated and nonirradiated group as references for the percentage analysis. All experiments were carried out in triplicate.

■ ASSOCIATED CONTENT

Supporting Information

The Supporting Information is available free of charge at https://pubs.acs.org/doi/10.1021/acsabm.1c00519.

Additional information on materials characterization and experimental procedures (PDF)

■ AUTHOR INFORMATION

Corresponding Author

Juliana Cancino-Bernardi − *Nanomedicine and Nanotoxicology Group, Physics Institute of São Carlos, University of São Paulo, São Paulo 13566-590, Brazil;* orcid.org/0000-0002-9584-2248; Email: jcancinobernardi@gmail.com

Authors

Olavo Santos − *Nanomedicine and Nanotoxicology Group, Physics Institute of São Carlos, University of São Paulo, São Paulo 13566-590, Brazil;* orcid.org/0000-0002-7752-0851

Paula Maria Pincela Lins − *Nanomedicine and Nanotoxicology Group, Physics Institute of São Carlos, University of São Paulo, São Paulo 13566-590, Brazil;* orcid.org/0000-0002-8663-4463

Diego Sampaio − *Nanomedicine and Nanotoxicology Group, Physics Institute of São Carlos, University of São Paulo, São Paulo 13566-590, Brazil; Innovation Group in Medical Instrumentation and Ultrasound (GIIMUS), Physics Department of the Faculty of Philosophy, Sciences and Letters of Ribeirão Preto, University of Sao Paulo, São Paulo 05508-220, Brazil;* orcid.org/0000-0002-3568-2828

Theo Pavan − *Innovation Group in Medical Instrumentation and Ultrasound (GIIMUS), Physics Department of the Faculty of Philosophy, Sciences and Letters of Ribeirão Preto, University of Sao Paulo, São Paulo 05508-220, Brazil;* orcid.org/0000-0002-9931-8558

Valtencir Zucolotto − *Nanomedicine and Nanotoxicology Group, Physics Institute of São Carlos, University of São Paulo, São Paulo 13566-590, Brazil;* orcid.org/0000-0003-4307-3077

Complete contact information is available at: https://pubs.acs.org/10.1021/acsabm.1c00519

Author Contributions

†O.S. and J.C.-B. contributed equally to this work.

Notes

The authors declare no competing financial interest.

■ ACKNOWLEDGMENTS

The authors are grateful to FAPESP, CAPES, and CNPq for the financial assistance. J.C.-B. thanks FAPESP process 2012/03570-0 and 2016/14303-3, PMPL thanks FAPESP process 2012/15630-7, T.Z.P. acknowledges FAPESP process 2013/18854-6. The authors thank LME/LNNano for technical support during the electron microscopy.

■ REFERENCES

(1) Tu, Y.; Cheng, K.; Shen, B.; Cheng, Z. Near-Infrared Fluorescence Nanoparticle-Based Probes: Application to in Vivo Imaging of Cancer. *Applications of Nanoscience in Photomedicine*Hamblin, M. R., Avci, P.; Chandos Publishing: Oxford, U.K., 2015; pp 131−151.

(2) Grossweiner, L. I.; Grossweiner, J. B.; Rogers, B. H. G. Phototherapy Light Sources. In *The Science of Phototherapy: An Introduction*; Springer, 2005.

(3) Jaque, D.; Martinez Maestro, L.; del Rosal, B.; Haro-Gonzalez, P.; Benayas, A.; Plaza, J. L.; Martin Rodriguez, E.; Garcia Sole, J. Nanoparticles for Photothermal Therapies. *Nanoscale* **2014**, *6* (16), 9494−9530.

(4) Menon, J. U.; Jadeja, P.; Tambe, P.; Vu, K.; Yuan, B.; Nguyen, K. T. Nanomaterials for Photo-Based Diagnostic and Therapeutic Applications. *Theranostics* **2013**, *3*, 152.

(5) Yang, X.; Yang, M.; Pang, B.; Vara, M.; Xia, Y. Gold Nanomaterials at Work in Biomedicine. *Chem. Rev.* **2015**, *115* (19), 10410−10488.

(6) Eustis, S.; El-Sayed, M. A. Why Gold Nanoparticles Are More Precious than Pretty Gold: Noble Metal Surface Plasmon Resonance and Its Enhancement of the Radiative and Nonradiative Properties of Nanocrystals of Different Shapes. *Chem. Soc. Rev.* **2006**, *35*, 209−217.

(7) Manivasagan, P.; Bharathiraja, S.; Bui, N. Q.; Jang, B.; Oh, Y.-O. O.; Lim, I. G.; Oh, J. Doxorubicin-Loaded Fucoidan Capped Gold Nanoparticles for Drug Delivery and Photoacoustic Imaging. *Int. J. Biol. Macromol.* **2016**, *91*, 578−588.

(8) Yoo, J.-W.; Chambers, E.; Mitragotri, S. Factors That Control the Circulation Time of Nanoparticles in Blood: Challenges, Solutions and Future Prospects. *Curr. Pharm. Des.* **2010**, *16* (21), 2298−2307.

(9) Ahmed, W.; Stefan Kooij, E.; Van Silfhout, A.; Poelsema, B. Controlling the Morphology of Multi-Branched Gold Nanoparticles. *Nanotechnology* **2010**, *21*, 125605.
(10) Tian, F.; Conde, J.; Bao, C.; Chen, Y.; Curtin, J.; Cui, D. Gold Nanostars for Efficient in Vitro and in Vivo Real-Time SERS Detection and Drug Delivery via Plasmonic-Tunable Raman/FTIR Imaging. *Biomaterials* **2016**, *106*, 87.
(11) Li, D.; Shi, X.; Jin, D. Polydopamine-Coated Gold Nanostars for CT Imaging and Enhanced Photothermal Therapy of Tumors. *Proc. SPIE* **2016**, *10013*, 100133L.
(12) Hao, F.; Nehl, C. L.; Hafner, J. H.; Nordlander, P. Plasmon Resonances of a Gold Nanostar. *Nano Lett.* **2007**, *7*, 729.
(13) Zhang, T.; Lu, G.; Shen, H.; Shi, K.; Jiang, Y.; Xu, D.; Gong, Q. Photoluminescence of a Single Complex Plasmonic Nanoparticle. *Sci. Rep.* **2015**, 3867.
(14) Cheng, L.; Wang, C.; Feng, L.; Yang, K.; Liu, Z. Functional Nanomaterials for Phototherapies of Cancer. *Chem. Rev.* **2014**, *114*, 10869.
(15) Song, C. Y.; Yang, B. Y.; Chen, W. Q.; Dou, Y. X.; Yang, Y. J.; Zhou, N.; Wang, L. H. Gold Nanoflowers with Tunable Sheet-like Petals: Facile Synthesis, SERS Performances and Cell Imaging. *J. Mater. Chem. B* **2016**, *4* (44), 7112−7118.
(16) Tiwari, P. M.; Bawage, S. S.; Singh, S. R. \Gold Nanoparticles and Their Applications in Photomedicine, Diagnosis and Therapy. *Applications of Nanoscience in Photomedicine*; Hamblin, M. R., Avci, P., Eds.; Chandos Publishing: Oxford, U.K., 2015; pp 249−266.
(17) Yuan, H.; Fales, A. M.; Vo-Dinh, T. TAT Peptide-Functionalized Gold Nanostars: Enhanced Intracellular Delivery and Efficient NIR Photothermal Therapy Using Ultralow Irradiance. *J. Am. Chem. Soc.* **2012**, *134*, 11358.
(18) Zhang, X. L.; Zheng, C.; Zhang, Y.; Yang, H. H.; Liu, X.; Liu, J. One-Pot Synthesis of Gold Nanostars Using Plant Polyphenols for Cancer Photoacoustic Imaging and Photothermal Therapy. *J. Nanopart. Res.* **2016**, 174.
(19) Lu, W.; Singh, A. K.; Khan, S. A.; Senapati, D.; Yu, H.; Ray, P. C. Gold Nano-Popcorn-Based Targeted Diagnosis, Nanotherapy Treatment, and in Situ Monitoring of Photothermal Therapy Response of Prostate Cancer Cells Using Surface-Enhanced Raman Spectroscopy. *J. Am. Chem. Soc.* **2010**, *132*, 18103.
(20) Lin, P. C.; Lin, S.; Wang, P. C.; Sridhar, R. Techniques for Physicochemical Characterization of Nanomaterials. *Biotechnol. Adv.* **2014**, *32*, 711.
(21) Xie, J.; Zhang, Q.; Lee, J. Y.; Wang, D. I. C. The Synthesis of SERS-Active Gold Nanoflower Tags for in Vivo Applications. *ACS Nano* **2008**, *2*, 2473.
(22) Qiao, Z.; Feng, H.; Zhou, J. Molecular Dynamics Simulations on the Melting of Gold Nanoparticles. *Phase Transitions* **2014**, *87* (1), 59−70.
(23) Chen, Y.-S.; Frey, W.; Kim, S.; Homan, K.; Kruizinga, P.; Sokolov, K.; Emelianov, S. Enhanced Thermal Stability of Silica-Coated Gold Nanorods for Photoacoustic Imaging and Image-Guided Therapy. *Opt. Express* **2010**, *18* (9), 8867.
(24) Sperling, R. A.; Rivera Gil, P.; Zhang, F.; Zanella, M.; Parak, W. J. Biological Applications of Gold Nanoparticles. *Chem. Soc. Rev.* **2008**, *37*, 1896−1908.
(25) Yun, S. H.; Kwok, S. J. J. Light in Diagnosis, Therapy and Surgery. *Nat. Biomed. Eng.* **2017**, *1*, 0008.
(26) Manivasagan, P.; Bharathiraja, S.; Bui, N. Q.; Jang, B.; Oh, Y. O.; Lim, I. G.; Oh, J. Doxorubicin-Loaded Fucoidan Capped Gold Nanoparticles for Drug Delivery and Photoacoustic Imaging. *Int. J. Biol. Macromol.* **2016**, *91*, 578−588.
(27) Park, J.; Ha, M. K.; Yang, N.; Yoon, T. H. Flow Cytometry-Based Quantification of Cellular Au Nanoparticles. *Anal. Chem.* **2017**, *89*, 2449.
(28) Habash, R. W. Y.; Bansal, R.; Krewski, D.; Alhafid, H. T. Thermal Therapy, Part 2: Hyperthermia Techniques. *Critical Reviews in Biomedical Engineering* **2006**, *34*, 491.
(29) Kuruvinashetti, K.; Kashani, A. S.; Badilescu, S.; Beaudet, D.; Piekny, A.; Packirisamy, M. Intracellular Localized Surface Plasmonic Sensing for Subcellular Diagnosis. *Plasmonics* **2018**, *13* (5), 1639−1648.
(30) Sohrabi Kashani, A.; Piekny, A.; Packirisamy, M. Using Intracellular Plasmonics to Characterize Nanomorphology in Human Cells. *Microsystems Nanoeng.* **2020**, *6* (1), 110.
(31) Ye, S.; Wheeler, M. C.; McLaughlan, J. R.; Tamang, A.; Diggle, C. P.; Cespedes, O.; Markham, A. F.; Coletta, P. L.; Evans, S. D. Developing Hollow-Channel Gold Nanoflowers as Trimodal Intracellular Nanoprobes. *Int. J. Mol. Sci.* **2018**, *19* (8), 2327.
(32) Vines, J. B.; Yoon, J. H.; Ryu, N. E.; Lim, D. J.; Park, H. Gold Nanoparticles for Photothermal Cancer Therapy. *Front. Chem.* **2019**, *7* (APR), 1−16.
(33) Shi, Y.; van der Meel, R.; Chen, X.; Lammers, T. The EPR Effect and beyond: Strategies to Improve Tumor Targeting and Cancer Nanomedicine Treatment Efficacy. *Theranostics* **2020**, *10* (17), 7921−7924.
(34) Ye, E.; Win, K. Y.; Tan, H. R.; Lin, M.; Teng, C. P.; Mlayah, A.; Han, M. Y. Plasmonic Gold Nanocrosses with Multidirectional Excitation and Strong Photothermal Effect. *J. Am. Chem. Soc.* **2011**, *133* (22), 8506−8509.
(35) Huang, P.; Rong, P.; Lin, J.; Li, W.; Yan, X.; Zhang, M. G.; Nie, L.; Niu, G.; Lu, J.; Wang, W.; Chen, X. Triphase Interface Synthesis of Plasmonic Gold Bellflowers as Near-Infrared Light Mediated Acoustic and Thermal Theranostics. *J. Am. Chem. Soc.* **2014**, *136* (23), 8307−8313.
(36) de Aberasturi, D. J.; Serrano-Montes, A. B.; Liz-Marzán, L. M. Modern Applications of Plasmonic Nanoparticles: From Energy to Health. *Adv. Opt. Mater.* **2015**, *3* (5), 602−617.
(37) Jo, H.; Youn, H.; Lee, S.; Ban, C. Ultra-Effective Photothermal Therapy for Prostate Cancer Cells Using Dual Aptamer-Modified Gold Nanostars. *J. Mater. Chem. B* **2014**, *2* (30), 4862−4867.
(38) Cabrelli, L. C.; Pelissari, P. I. B. G. B.; Deana, A. M.; Carneiro, A. A. O.; Pavan, T. Z. Stable Phantom Materials for Ultrasound and Optical Imaging. *Phys. Med. Biol.* **2017**, *62*, 432.

https://doi.org/10.1021/acsabm.1c00519
ACS Appl. Bio Mater. XXXX, XXX, XXX−XXX